CrossMark

Mineral colloids mediate organic carbon accumulation in a temperate forest Spodosol: depth-wise changes in pore water chemistry

Ekaterina Bazilevskaya · Douglas D. Archibald · Carmen Enid Martínez

Abstract Mobile submicron mineral phases within soil pore waters are presumed to play a major role in the transport and availability of organic carbon (OC) in subsurface horizons. This work reports on the composition of the < 0.45 μm and 0.45–1.2 μm size fractions of extracted soil pore waters from horizons of a well-drained-Spodosol-soil to reveal conditions favorable for carbon mobility and accumulation. These operationally defined quantities are abbreviated SF-S (size fraction small) and SF-L (size fraction large) to identify the < 0.45 μm and the 0.45–1.2 μm size fraction filtrates, respectively. It is found that in the SF-S fraction, OC mass concentrations are more than 30–50 times higher than metal (M = Fe + Al) mass concentrations in all Spodosol horizons, with metal-to-carbon (M/C) atomic ratios of 0.15–0.03. Chemical equilibrium modeling calculations estimate $> 95\%$ of the total Fe and Al in SF-S are complexed with OC in all Spodosol horizons. In contrast with the SF-S, the SF-L had much greater OC concentrations and even lower M/C (< 0.01), except in the Bh horizon (M/C = 0.05). In Bh, major accumulation of organic matter occurred above the lesser-accumulating Bhs, the latter having higher pH, but much lower OC in all forms (soil, colloidal). Infrared spectroscopy indicates the SF-L fraction of soil pore waters contains both organic and inorganic constituents, including amorphous silica, the second-most abundant component after OC. Mineral-organic associations such as mineral crystallites embedded in OC are observed in the SF-L fraction by transmission electron microscopy (TEM). Transmission electron microscopy also reveal carbon-rich amorphous structures containing traces of Fe, Al and Si, and small (~ 100 nm) spherical amorphous SiO_2 particles. These observations provide support for the main mechanism of OC accumulation in Spodosols being the downward movement of colloids (organic, OC-sorbed mineral and organo-mineral), followed by colloid immobilization due to a combination of increases in pH and M/C ratio. The occurrence of these three types of colloidal structures in pore waters

Responsible Editor: Stephen D. Sebestyen.

C. E. Martínez (✉)
Soil and Crop Sciences, School of Integrative Plant Science, SIPS, Cornell University, 906 Bradfield Hall, Ithaca, NY 14853, USA
e-mail: cem20@cornell.edu

E. Bazilevskaya
Materials Characterization Laboratory, The Pennsylvania State University, University Park, PA 16802, USA

D. D. Archibald
Department of Ecosystem Science and Management, The Pennsylvania State University, University Park, PA 16802, USA

seems to depend on the pH and the relative supply of OC and Fe + Al to pore waters. Similar colloidal structures might also contribute to the transport and availability of OC in subsurface horizons of soils that range in the accumulation of organic and organo-metallic compounds, that is, in the expression of spodic properties.

Keywords Colloids · Soil pore waters · Organic carbon · Soil · Spectroscopy · Microscopy

Introduction

Carbon stabilization in subsurface soil horizons cannot be solely attributed to the chemical structure of organic matter (OM); rather, OM sorption onto soil mineral phases, the formation of OM-mineral co-precipitates and metal-OM complexes, in addition to physical occlusion are all postulated to contribute to carbon stabilization and preservation in soils (Lützow et al. 2006; Wagai and Mayer 2007; Kaiser and Kalbitz 2012; Kleber et al. 2015; Bernal et al. 2016; Han et al. 2016). NMR studies, for example, have found that ∼ 90% of deep organic carbon (OC) is physically and/or chemically associated with soil minerals (Golchin et al. 1994; Christensen 1996). The formation of these mineral-organic associations (MOA) decreases carbon mineralization rate thus increasing carbon reserves in soil (Riise et al. 2000; Tan 2003; Pokrovsky et al. 2005; Tolpeshta and Sokolova 2009; Lalonde et al. 2012; Camino-Serrano et al. 2014; Chen et al. 2014; Vogel et al. 2014; Kleber et al. 2015; Vindedahl et al. 2016; Rasmussen et al. 2018).

Sorption of OC onto highly reactive, poorly crystalline mineral phases is considered one of the major factors that controls OC accumulation and stability in subsurface soil horizons of acidic soils (Kramer et al. 2012). The clay particle-size fraction (< 2 μm), that includes different forms of metallic oxyhydroxides and poorly crystalline aluminosilicates, most efficiently protect organic matter from mineralization (Jones and Edwards 1998; Dignac et al. 2017) while the resistance to microbial degradation of OC within MOA depends on the structure and crystallinity of associated mineral phases (Wagai and Meyer 2007; Basile-Doelsch et al. 2015; Kramer et al. 2017).

Forest soils, such as Spodosols, are characterized by intensive transport of organic matter, Fe and Al hydroxides and clay minerals through the soil profile, and by their accumulation in subsurface horizons (De Coninck 1980; Duchaufour 1982; Farmer and Frazer 1982; Buurman and van Reeuwijk 1984; Kartlun et al. 2000). Two major competitive theories of Spodosol formation have been proposed (Schaetzl and Anderson 2005). In the first, the proto-imogolite theory, silicate mineral weathering results in the downward transport of Fe, Al and Si in the form of polymeric Fe–Al–Si inorganic components (imogolite) which are immobilized in subsoils due to changes in pH. Negatively charged organic colloids then precipitate onto (or react with) the positively charged surfaces of imogolite (Farmer and Frazer 1982; Kartlun et al. 2000). The second theory, the chelate theory, postulates that Fe, Al, and Si form metal–organic complexes that are highly mobile and freely move down the profile along with percolating waters. Precipitation of metal–organic complexes then occurs in the B horizon due to saturation of the complexing capacity of the organic molecules (McKeague et al. 1971; Van Hees and Lundstrom 2000). The mobilization and translocation mechanisms presumed to be involved in Spodosol formation implicate the following chemical processes: (1) formation of stable water-soluble complexes of organics with Fe, Al, and Si (Buurman and van Reeuwijk 1984; De Coninck 1980; Duchaufour 1982); (2) reduction of Fe in aluminosilicate clays by organic acids and migration of stable Fe(II)-organic complexes (Bloomfield 1953; Sklemdtad 1992); and (3) hydrolysis of Al, Si, and Fe to form stable inorganic colloidal sols (Farmer 1974; Farmer and Frazer 1982). The accumulation (immobilization) of Al, Si and Fe in lower illuvial horizons has been explained by precipitation of Fe and Al with silica as allophanic material, by precipitation of metal–organic complexes due to increase in (Fe + Al) to C ratios in organic complexes, and by microbial decomposition of metal–organic complexes with further precipitation of Fe and Al hydroxides (De Coninck 1980; Schnitzer et al. 1984). Direct evidence of dominant mobilization, translocation, and immobilization mechanisms is still incomplete, as is the identification of the presumed types of colloidal structures present in pore waters. These mechanisms are however proposed to depend on the dynamics of organic matter within the Spodosol profile (Buurman and Jongmans 2004).

Highly reactive organic acids released from coniferous vegetation hampers crystallization and growth of secondary minerals. These secondary minerals, for example permanently charged phyllosilicate clay minerals and variably charged nanometer-sized Fe minerals, are very reactive with respect to OC sorption (Lundström et al. 2000; Jansen et al. 2003; Buurman and Jongmans 2004; Eusterhues et al. 2008; Basile-Doelsch et al. 2015). The organic matter that migrates to subsurface horizons is also small and mobile (Rumpel and Kögel-Knabner 2011). Therefore, dominant structures involved in OC transport-accumulation through soil profiles are expected to occur within the dissolved and colloidal size fractions of soil pore waters.

As defined by Sposito (1989), "the characteristic property of colloids is that they do not dissolve in water to form solutions, but instead remain as an identifiable solid phase in suspension". Colloids are also defined as inorganic or organic particles with sizes ranging from 1 nm to 1 μm (Buffle et al. 1998), which correspond to the fine clay size fraction (Schoenberger et al. 2002). In most experimental studies, colloids are operationally defined (e.g., > 0.7 μm, > 0.45 μm, low molecular weight (10–1 kDa), high molecular weight (0.22 μm–10 kDa), etc.) depending on the extraction techniques used (Gustafsson 2009; Hirst et al. 2017; Oleinikova et al. 2017) and on the field of study. More generally, a colloid is any constituent small enough, that remains well-dispersed in soil waters within substantial periods of time (from hours to days), and that has enough surface area to adsorb other chemicals (Gustafsson 2009). The stability of soil colloids is determined by factors that promote or prevent their aggregation (Buffle et al. 1998). The colloidal fraction is the most mobile in soil waters, while macro-particles (or large aggregates) are rapidly removed from soil waters by gravity (Wen et al. 2008).

Strong interactions among Al, Si, Fe and mineral and organic phases make Spodosols a soil of choice to study the role mineral colloids might have on carbon stabilization and transport. While interactions between OM and Al and Fe are recognized to contribute to the stability of soil OM in subsurface Spodosol horizons (Riise et al. 2000; Nierop et al. 2002; Chen et al. 2014), detailed understanding of these structures, of their interactions at the submicron scale in soil pore waters,

and of their role on carbon transport-accumulation as a function of soil depth is still incomplete.

This work provides a thorough baseline chemical and physical characterization of five horizons of a temperate forest Spodosol that is prevalent in North America. We then focus on the operationally defined < 0.45 μm size fraction (abbreviated SF-S, size fraction small) and 0.45 μm to 1.2 μm size fraction (abbreviated SF-L, size fraction large) of extractable soil pore waters from each of the horizons. The specific goals are as follow: (i) to elucidate the composition of soil pore waters and their colloidal structures, (ii) to determine whether these colloidal structures change with soil depth, and (iii) to reconstruct the most likely pathways for the short-term translocation and immobilization of mineral and organic colloids in this type of soil. More generally, we seek to understand the role of mineral colloids in translocation and immobilization of organic carbon by investigating the type of associations by which translocation of organic carbon occurs in both the SF-L and SF-S size fractions. We hypothesize that various mobile structures, including metal–organic complexes and colloids and mineral-organic associations, are present in soil pore waters (SF-S and SF-L) and mediate organic matter translocation and accumulation with depth. We further hypothesize that immobilization of organic carbon occurs along with transformation/evolution of metal species within the soil profile (i.e., from metal to organic complexation to heterogeneous precipitation), where the composition of mineral-organic associations, specifically their $(Fe + Al)/C$ ratio, becomes more important in the 0.45–1.2 μm (SF-L) size fraction. We test these hypotheses by combining sensitive spectroscopic and microscopic analyses with chemical equilibrium modeling. Understanding the structures and behavior of mineral-organic associations is helpful in predictions of the long-term retention of organic matter in soils that reflect patterns that drive ecosystem functioning.

Materials and methods

Site description and soil characterization

The spodosol site chosen for this study is located in Black Moshannon State Forest in Central Pennsylvania (40°53′22.28″N, 78°02′24.82″W) on the level

upland position (0–3% slopes) of the Allegheny Plateau. The soil is classified as an Entic Haporthod, from the Leetonia series. The site is covered by coniferous vegetation (hemlock, *Tsuga Canadensis*) and underlain by sandstones of the Mississippian Ponoco formation. At this location, the mean annual air temperature (MAAT) is approximately 10 °C, and the mean annual precipitation (MAP) is about 1145 mm/year (Ciolkosz and Thurman 1992).

Five soil horizons were identified and characterized at this site (Table 1): *AO* (partially decomposed organic matter, OM), *E* (strongly leached, light colored), *Bh* (subsoil, accumulation of humus), *Bhs* (subsoil, accumulation of humus and sesquioxides), and *C* (slightly altered, similar to parent rock). Although the Leetonia series are typically described to have a Bh but not a Bhs horizon, we found evidence for the presence of a Bhs horizon (Table 1). Each soil horizon was analyzed for total carbon and nitrogen content, pH, mineralogy of the clay size fraction, and by selective extractions of crystalline (dithionate-citrate extractable), amorphous (ammonium oxalate-extractable, in the dark) and organic (Na-pyrophosphate extractable) forms of Fe and Al. A small sample of 3–4 mm intact soil aggregates from horizons E, Bh and Bhs was characterized using micro computed tomography (μ-CT). Details on selective extraction procedures and X-ray diffraction analyses can be found in Online Appendices A and B, respectively.

Collection and analyses of soil pore waters

A variety of soil pore water sampling techniques exists, however, no one single methodology is appropriate for all applications and the choice of the technique therefore depends on the aim of the study and the properties of the soil (Sigfusson et al. 2006; Orlowski et al. 2016; Di Bonito et al. 2018). In this work, pore water extraction experiments were designed for sandy soils which do not normally hold large amounts of water when field-moist and have narrow (5–20 cm) and uneven soil horizons; under these conditions, the use of field extraction techniques (e.g., lysimeters) to obtain pore water from each horizon is challenging. The purpose of these experiments was to simulate a rain event in the laboratory that would mobilize colloids in water-saturated soils and to compare relative differences (not absolute quantities) in the characteristics of pore waters among soil horizons. To collect soil horizons from the field with minimum disturbance of soil structure, the soil horizons were carefully augered in-place using in-house-built round sample holders (height, 44 mm; diameter, 64 mm) cut from chemically inert PVC tubes. We observed no breakage of soil agglomerates during this procedure. The soil-containing rings were immediately sealed with parafilm to prevent drying and stored at 4 °C. Each soil horizon (in PVC sample holder) was placed in a filtration apparatus (Online Appendix C, Fig. C1), rewetted to field capacity (i.e., to the amount of water left in the soil after excess water has been drained by gravity) and allowed to equilibrate for 24 h at 4 °C. The field capacity was determined in preliminary experiments to be 50, 20, 25, 25 and 20% water for the AO, E, Bh, Bhs and C horizons, respectively. The filtration apparatus with field-collected soils was then connected to a vacuum line with 5-10 psig of vacuum pressure for 30 min to obtain soil pore waters. The applied vacuum pressure was low enough and comparable to the water tension at field capacity (4.8 psi) to exclude the possibility of soil disturbance. Two separate water extractions were carried out for each horizon. The first used a filtration apparatus with 0.45 μm pore size cellulose acetate filters to collect the SF-S size fraction (i.e., soil water < 0.45 μm). The second used a filtration apparatus with 1.2 μm glass fiber (grade 696) pore size filters to collect the SF-L size fraction (< 1.2 μm). The SF-L fraction also includes the SF-S fraction, but later in this report we show that the mass concentration of the SF-S fraction is generally much smaller than the SF-L fraction, which also assures the extracted core behaved like an undisturbed core. All filters were prewashed 3 times with de-ionized purified water. The extracted soil pore waters were stored at 4 °C or freeze-dried for infrared analyses. A portion of the soil waters (from < 0.45 to < 1.2 μm filtrates) was acidified by addition of HCl, and total Fe, Al and Si determined by inductively coupled plasma atomic emission spectroscopy (ICP-AES). The SF-L fraction concentrations presented in Fig. 1 were calculated by subtracting total ICP-determined concentrations in the SF-S fraction from the total ICP-determined concentrations in < 1.2 μm filtrates.

Dissolved organic carbon (DOC), operationally defined as the organic carbon in soil water that passes through a 0.45 μm pore size filter (Thurman 1985), was determined in non-acidified filtrates using a

Table 1 Soil horizons in the Black Moshannon Spodosol site

Horizon	Depth (cm)	Properties	Soil pH H_2O:soil = 3:1	Total C %	Total N %	Minerals in < 2 μm size fraction	Fe crystalline/ Fe amorphous/Fe organic (g/kg)	Al amorphous/ Al organic (g/kg)	% amorphous material[a]
AO	0–15	Brown, loamy sand, weak granular structure, non-sticky, abrupt boundary, many fine and thick roots from the trees, partially decomposed organic residues	3.4	23.28 ± 2.46	0.84 ± 0.25	Q, K, Ilt[b]	1.58 ± 0.10/ 0.75 ± 0.18/ 0.14 ± 0.12	0.18 ± 0.05/ 0.63 ± 0.04	0.29
E	15–25	Light gray, loamy sand, single-grained, non-sticky, abrupt wavy boundary	3.9	0.23 ± 0.02	0.01 ± 0.01	Q, K, Ilt	0.40 ± 0.009/ 0.02 ± 0.00/ 0.00 ± 0.00	0.01 ± 0.01/ 0.02 ± 0.01	0.01
Bh	25–30	Strong brown, sandy loam, weak, fine granular structure, friable, non-sticky, diffuse wavy boundary	3.8	3.01 ± 0.23	0.14 ± 0.01	Q, K, Ilt, Ve	8.75 ± 0.056/ 7.38 ± 0.03/ 0.59 ± 0.01	1.31 ± 016/ 4.70 ± 010	2.67
Bhs	30–50	Reddish-yellow, sandy loam, medium sub-angular blocky structure, slightly sticky, gradual boundary	4.1	0.36 ± 0.03	0.04 ± 0.01	Q, K, Ilt, Ve	7.59 ± 0.82/ 1.50 ± 0.06/ 0.16 ± 0.01	0.20 ± 0.10/ 2.40 ± 0.17	0.58
C	50–84	Olive-yellow, loamy sand, single-grained, medium to fine platy structure, non-sticky, gradual boundary	4.3	0.11 ± 0.02	0.01 ± 0.01	Q, K, Ilt, Ve	0.83 ± 0.05/ 0.25 ± 0.02/ 0.03 ± 0.00	0.04 ± 0.04/ 1.00 ± 0.01	0.12

Morphology standards used are given by Schoenberger et al. (2002)

[a] Includes amorphous and poorly-crystalline forms of Fe, Al and Si determined from ammonium oxalate extraction in the dark

[b] Mineral notation: Q—quartz, K—kaolinite, Ilt—illite, Ve—vermiculite
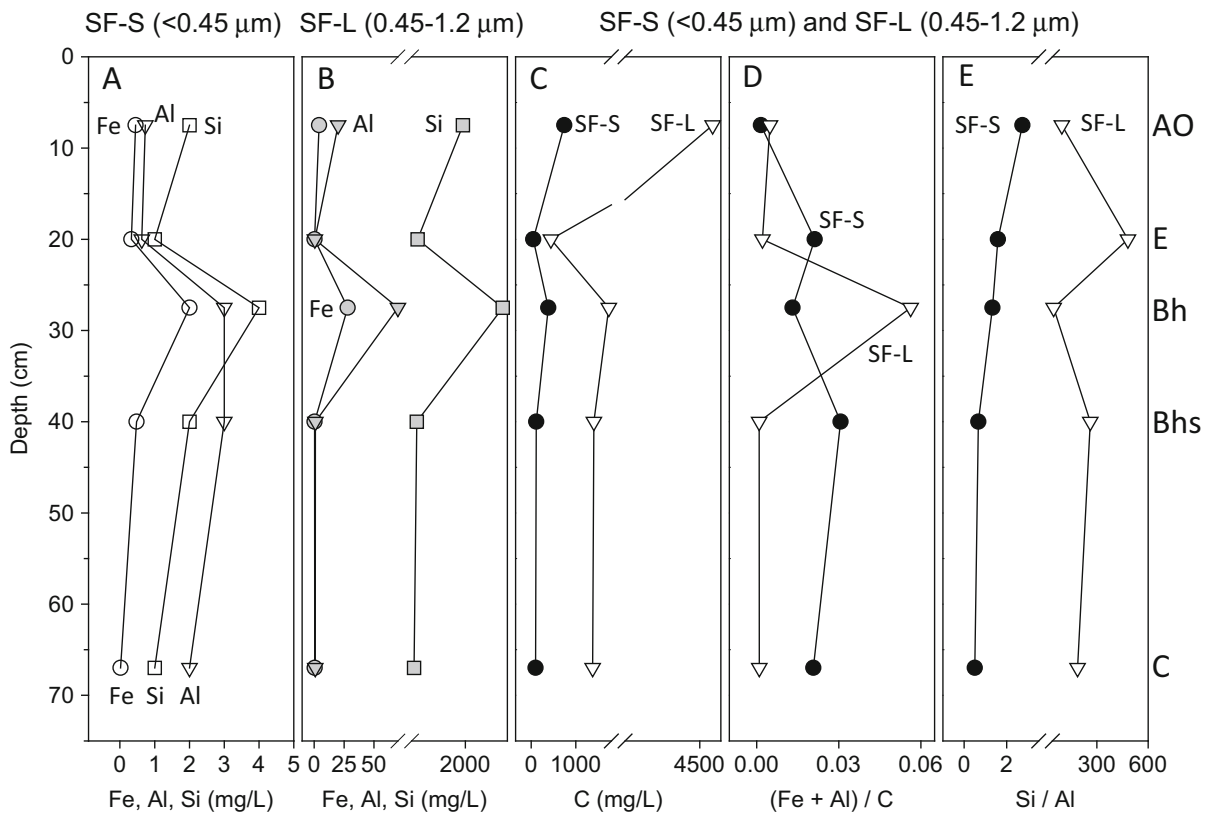
Fig. 1 Elemental concentrations and ratios in soil pore water fractions of Spodosol horizons. Concentrations of Fe, Al and Si in the **a** SF-S (< 0.45 µm) and **b** SF-L (0.45–1.2 µm) fractions; **c** organic carbon concentrations in the < 0.45 µm and the 0.45–1.2 µm size fractions; and **d** (Fe + Al)/C and **e** Si:Al atomic ratios present in the SF-S and SF-L fractions of soil pore waters

SHIMADZU TOC-5000A total organic carbon analyzer. A measure of colloidal organic carbon (COC) was obtained by filtration of the < 1.2 µm soil water fraction through a 0.45 µm pore size Millipore silver (Ag) filter. The carbon retained on the 0.45 µm silver filter is defined as colloidal organic carbon (COC). Silver filters were used because of their low carbon concentration and availability of small pore size diameter (0.45 µm). The silver filters were pre-treated by heating in a furnace at 300 °C for 30 min to remove any trace amounts of carbon, and oven dried at 60 °C for 1 h to remove moisture. No detectable carbon was measured on blank filters. Before filtration of soil waters, each filter was washed 3 times with 5 mL of purified water. To collect the colloidal organic carbon fraction, 1 mL of the < 1.2 µm soil water fraction was passed through a 0.45 µm pore size silver filter, which was then dried at 60 °C for 1 h. The mass of material retained on the filter was estimated as the difference

between the weights of the dried filter after and before filtration. The carbon content of the filters (i.e., COC) was determined using an EA 1110 CHNS-O analyzer (CE Instruments), with a detection limit of 0.1 mg/L and an uncertainty of 0.02 mg/L.

The Attenuated Total Reflectance Fourier Transform Infrared (ATR-FTIR) spectra of the SF-S (< 0.45 µm) and SF-L (< 1.2 µm) water fractions were collected using a Bruker Tensor 27 FTIR instrument equipped with a diamond Zn–Se ATR sensor. To increase the intensity of the infrared spectra, 1 mL of soil water was placed in 1.6 mL glass vials, freeze-dried, and reconstituted in 0.05 mL of Milli-Q water. Three laboratory replicates for each sample set and blanks were prepared. A 0.5 µL aliquot of the reconstituted soil water extract was placed on the sensor and dried to form a thin coating before data collection; each aliquot was measured twice. Drying and data collection were done under an argon gas

atmosphere. The spectra were collected in the 4500–600 cm^{-1} region with an 8 cm^{-1} resolution and co-addition of 128 rapid scans. The ATR-FTIR spectra of mineral and organic standards (illite, vermiculite, kaolinite, silica and humic acid) were also collected and used for the identification of components (fingerprints) in the spectra of soil waters.

The material collected on the 0.45 μm silver filters (i.e., colloids ranging in size between 0.45 and 1.2 μm) was observed using a Hitachi scanning electron microscope (SEM; S-3500 N). Images were collected in low vacuum (20 kPa) to avoid electron charging of non-coated samples. The elemental composition of the colloids present on the filter was determined from secondary electrons using energy-dispersive X-ray spectroscopy (EDS; Princeton Gamma Tech). An image of a blank silver filter was also collected. For each filter, 5–8 areas ($\sim$ 100-μm^2 size) and 2–4 spot measurements per area were analyzed by EDS. In addition, samples for transmission electron microscopy (TEM) were prepared by placing a single drop of soil water (< 1.2 μm size fraction) onto a TEM holey carbon-coated copper grid and allowed to air-dry. No sample dilution was performed. TEM images, EDS spectra, and selected area electron diffraction (SAED) patterns were collected using a JEOL TEM-2010 with a LaB$_6$ (lanthanum hexaboride) filament operated at 200 kV.

Chemical equilibrium modeling calculations

Visual MINTEQ (Gustafsson 2009) is used to calculate the speciation of Fe and Al in the presence of DOC for all horizons. The calculations are based on total concentrations of Fe and Al, pH, and DOC measured in this work (< 0.45 μm fraction). Additional cations and anions in a similar Spodosol soil (Shepard et al. 1990) are included in the calculation to maintain charge balance; charge difference in general did not exceed 10%. The NICA-Donnan humic ion binding model (Milne et al. 2003) within Visual Minteq is used to describe cation interactions with dissolved organic acids.

A second modeling approach is used which involves the complexation of Al and Fe with catechol-type groups in solutions saturated with respect to the precipitation of Fe and Al hydroxides. Catechol is selected because it represents a functionality abundant in soil organic matter and because it is considered an important functional group involved in the formation of Al(III) and Fe(III) complexes with OM (Erich and Trusty 1997; Tipping 2002). The overall dissociation constant, K$_{diss}$, for the reaction: LH$_2$ (phenol) = L^{2-} (phenolate) + 2H$^+$ equals $10^{-22.23}$. The stability constants, K$_{ML}$, for metal-catechol complexation in solution (K$_{ML\text{-}Al}$ = $10^{16.3}$, K$_{ML\text{-}Fe(III)}$ = 10^{20}) are taken from Schweigert et al. (2001). The model organic matter concentration, L$_T$, is set to contain 100 mmol/kg of catechol groups, representing the maximum complexing capacity for this organic material (McBride 1994). The following equation, where M is metal (Fe or Al) concentration, was modified to calculate the concentration of metal-catechol complexes (ML):

$$K_{diss}K_{ML} = \frac{ML}{(L_T - ML)}\frac{(H^+)^2}{M}$$

Results

Soil characteristics

All soil horizons in the Spodosol profile have an acidic pH that increases slightly with depth from 3.4 in the AO horizon to 4.3 in the C horizon; the clay fraction is dominated by illite and kaolinite as determined by XRD (Table 1). As expected, the highest concentrations of total carbon are found in the AO (23%) and Bh (3%) horizons. All horizons show greater amounts of Fe in crystalline form, followed by amorphous and then organic forms of Fe. In contrast, organic forms of Al dominated over amorphous Al in all horizons. The Bh and Bhs horizons contain the greatest concentrations of crystalline and amorphous forms of Fe, and of organically-bound Al. In particular, the Bh and Bhs horizons contain more organically-bound Al than Fe, thus indicating subsurface accumulation of organic carbon in association with aluminum. The total amount of amorphous material associated with Fe, Al and Si is highest in the Bh horizon. Images of undisturbed soil aggregates (3–4 mm size) obtained by μ-computed tomography (μ-CT) show the accumulation of particulate organic matter in the Bh horizon and cementation of quartz particles in the Bhs horizon, presumably by Fe and Al hydroxide

precipitates and organic coatings (Online Appendix D, Fig. D1).

Carbon, Fe, Al and Si in soil pore waters

The concentrations of SF-S (< 0.45 μm fraction) and SF-L (< 1.2 μm fraction) Si, Al and Fe in soil pore waters present similar trends with depth (Fig. 1a, b), with elemental concentrations in the SF-L fraction higher than in the SF-S fraction. Furthermore, all three elements have their maximum concentrations in pore waters extracted from the Bh horizon. The concentration of Fe is generally lower than that of Al, while Si concentrations are typically 100–400 times higher than that of Al, except in the SF-S fraction of the Bhs and C horizons. Organic carbon (OC) concentrations (SF-S and SF-L) are highest in pore water extracts from the AO horizon and lowest from the E horizon; these concentrations however increase further in pore waters collected from the Bh horizon (Fig. 1c). SF-S and SF-L concentrations of organic carbon are on average 60–100 times higher than corresponding concentrations of Al, Fe and Si in all spodosol horizons (Fig. 1d). Although the (Fe + Al)/C ratio is generally lower in the SF-L than in the SF-S fraction, a dramatic increase in the SF-L (Fe + Al)/C ratio is observed in pore water extracted from the Bh horizon, corresponding with the highest concentrations of crystalline, amorphous and organically-bound forms of Fe and Al (Table 1). The Si:Al ratios in the SF-S fraction decrease gradually from 3 in the AO horizon to 0.5 in the C horizon (Fig. 1e). The SF-L fraction shows a Si:Al ratio of 480 in the E horizon and of ~ 200 in the Bhs and C horizons; lower ratios are present in the AO and Bh horizons (i.e., higher Al concentrations).

Analyses of pore water DOC by chemical equilibrium modeling

Chemical equilibrium modeling calculations utilizing actual metal and DOC concentrations from pore water of each horizon estimate that 95% and $> 95\%$ of the total Al and Fe in SF-S fraction, respectively, exist in complexes with DOC (i.e., aqueous Al-DOC and Fe-DOC complexes). Additionally, catechol-method calculation results show that in the pH range of Spodosol waters (3.4–4.3), more than 90% of both Fe and Al are expected to complex with catechol-type functional groups.

ATR-FTIR spectra of soil pore waters

The ATR-FTIR spectra of soil pore water samples and reference mineral and organic specimens are presented in Fig. 2; a compilation of peak assignments is available in Online Appendix E, Table E1. FTIR spectra of the SF-S (< 0.45 μm) and SF-L (< 1.2 μm) fractions of soil pore waters show vibrations indicative of both mineral and organic components; in particular, peaks associated with prominent organic functional groups (Fig. 2). The later include stretching (v) O–H/N–H at ≈ 3400 cm^{-1}; asymmetric and symmetric aliphatic CH$_2$ stretching at ≈ 2920 and ≈ 2850 cm^{-1} (respectively); C=O/COOH stretching at ≈ 1730–1720 cm^{-1}; asymmetric COO– stretching at ≈ 1645–1640 cm^{-1}; symmetric COO– stretching at ≈ 1435–1430 cm^{-1}; ester/phenolic C–O stretching at ≈ 1326–1310 cm^{-1}; aliphatic C–C/C–O–C stretching at ≈ 1110–1035 cm^{-1} (Chorover and Amistadi 2001; Parikh et al. 2014). It is likely structures containing aromatic C=C stretching vibrations (at ≈ 1513 cm^{-1}) are present in extracted soil pore waters, however, these features might have been obscured by the presence of more abundant COO- functionalities. Mineral components show sharp peaks below 1200 cm^{-1}, so that the peaks at 1110 and 1035 cm^{-1} may also be attributed to asymmetric Si–O stretching of silica (1110 cm^{-1}) and kaolinite (1035 cm^{-1}) (Fig. 2).

The SF-L fraction (< 1.2 μm) of the A, E, Bhs, C, and to a lesser extent the Bh horizons shows vibrations at 2920 and 2850 cm^{-1} that are assigned to aliphatic CH$_2$ stretching vibrations (Fig. 2b). Also present in the SF-L fraction from all horizons are peaks at ≈ 1645 and ≈ 1430 cm^{-1}, which are assigned to carboxylate (COO$^-$) asymmetric and symmetric stretching vibrations, respectively. Carboxylate functional group binding to metal ions or mineral surfaces results in relative increases in intensity of these vibrations (Allard et al. 2002). A shoulder located at ≈ 1732 cm^{-1} is assigned to C=O/COOH stretching vibrations of carboxylic groups (Hay and Myneni 2007); this vibration is most prominent in the AO and Bh horizons. An additional shoulder is most prominently observed in the E, Bhs and C horizons, attributed to ester/phenolic C–O stretching

Fig. 2 ATR-FTIR spectra of soil pore water fractions from the AO, E, Bh, Bhs and C Spodosol horizons. Panel **a** SF-S fraction (< 0.45 μm) and panel **b** SF-L fraction (< 1.2 μm). The spectra of reference materials are also shown. HA, humic acid
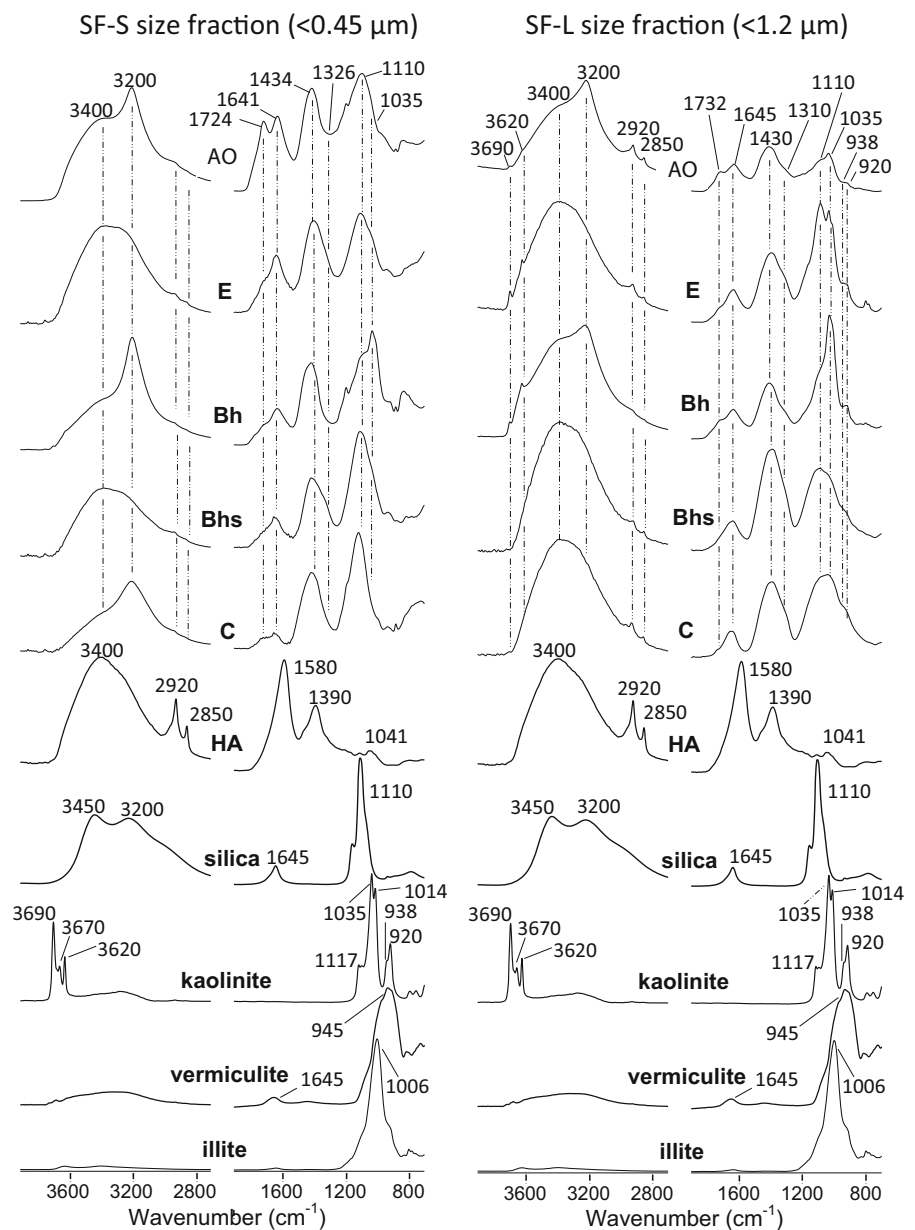
at ≈ 1310 cm^{-1}. Vibrations resulting from aliphatic C–C/C–O and C–N bonds are present in the ≈ 1200–950 cm^{-1} region of all horizons (Gu et al. 1995; Tan 2003; Oren and Chefetz 2012). The FTIR spectra of the SF-S fraction (< 0.45 μm) also show peaks attributed to organic constituents (Fig. 2a). The most striking differences between the SF-S and SF-L fractions are a much lower intensity resulting from C–H stretching vibrations in the SF-S fraction, and particularly in water collected from the

AO horizon, stronger vibrations in the carboxylate (1641 cm^{-1}), carboxylic (1724 cm^{-1}), and C–O and C–N (≈ 1110–1035 cm^{-1}) regions of the spectra (Fig. 2a).

The presence of mineral phases in the SF-L fraction is revealed by vibrations at 3690 and 3620 cm^{-1} in the spectra from the E, Bh, and to a lesser extent the AO horizons, which are attributed to O–H stretching vibrations in kaolinite (Fig. 2b, Online Appendix Table B1). Illite and/or chlorite would also have a

peak at ≈ 3600 cm^{-1}, but not as sharp as the one from well-crystallized kaolinite (Farmer 1974). In addition, the spectra for the AO and Bh horizons exhibit a relatively sharp peak at 3200 cm^{-1}, which represents OH stretching vibrations due to the presence of colloidal silica (Bailey and McGuire 2007). The presence of mineral phases in the SF-L fraction is further confirmed by sharp IR vibrations in the fingerprint region of the A, E and Bh horizons (Fig. 2b); these vibrations are also present in the Bhs and C horizons, although not as sharp, and may also result from the presence of organic constituents. Relatively sharp peaks at ≈ 1100–900 cm^{-1} are assigned to Si–O stretching vibrations of colloidal silica (Bailey and McGuire 2007), allophane (Madejova 2003), imogolite (Kartlun et al. 2000) or kaolinite. We therefore assign vibrations at 1035 cm^{-1} and 1110 cm^{-1} in the A, E and Bh horizons to the presence of colloidal kaolinite and silica with poorly-crystalline aluminosilicates. Although kaolinite and silica may contribute to the intensity of the 1110 cm^{-1} (silica) and 1035 cm^{-1} (kaolinite) vibrations in the SF-L water fraction of the Bhs and C horizons, the ≈ 3700–3600 cm^{-1} and 3200 cm^{-1} vibrations would have been clearly evidenced if these minerals alone contributed to these vibrations (Fig. 2b). Except for weak vibrations in the Bh horizon, the FTIR spectra of the SF-S fraction (Fig. 3a) lack the characteristic kaolinite peaks at ≈ 3700–3600 cm^{-1}, however, prominent Si–O–Si stretching vibrations (3200 cm^{-1}) are present in the A, Bh and C horizons. These observations suggest the presence of poorly-crystalline Si nanoparticles that passed through the 0.45 μm pore size filter.

In the SF-L fraction, the relative proportion of mineral phases increases from the AO to the Bh horizons whereas that of organic constituents decreases. The FTIR spectra of the SF-L fraction of the Bhs and C horizons is however attributed mainly to organic components. Vibrations attributed to organic molecules seem to prevail in the SF-S fraction, with the presence of colloidal silica in the A, Bh, and to a lesser extent in the C horizon. No crystalline Fe minerals are identified in any of the soil water extracts, and ferrihydrite is not detected by IR because it produces only a broad peak in the 3600–3200 cm^{-1} region (Table B1). Overall, IR analyses reveal the strong presence of organic materials, as well as the association of kaolinite and colloidal silica in both the SF-S and SF-L size fractions.

Analyses of the 0.45–1.2 μm size fraction (SF-L) of soil pore waters by electron microscopy and energy dispersive X-ray spectroscopy

Analyses by scanning electron microscopy (SEM) and energy dispersive X-ray spectroscopy (EDS) show soil pore water colloids (0.45–1.2 μm fraction) present a diversity of morphologies (Fig. 3a) and a wide range in the distribution of Al, Fe and C concentrations (Fig. 3b). Approximately 90% of observed colloids from the AO horizon exhibit an amorphous appearance with some fibrous features typical of organic materials. In the Bh horizon a significant portion of the colloids consist of 0.5–1.5 μm round particles containing C, Al, Si, Fe and traces of Mg embedded in a darker C-rich matrix. Ugolini et al. (1977) have also observed 0.5–1.5 micron oblong, ellipsoidal or spherical organo-mineral particle aggregates by SEM in 0.1 μm filter residues of Spodosol soil solutions. Colloids from the Bhs horizon appear featureless, however some areas contain occasional particles with elevated Fe content ($\sim$ 6% Fe vs. 2% Fe on average).

Analyses using EDS indicate the magnitude and range of concentrations of Al and Fe in pore water colloids increase with depth from the AO to the Bh and Bhs illuvial horizons (Fig. 3b). Specifically, Al concentrations in water colloids from the AO horizon are below 2.5 at.%, increase to $\sim$ 5 at.% in the Bh horizon, and reach a value of up to 40 at.% Al in the Bhs horizon with a highly heterogeneous distribution of concentrations (2–40 at.%). Iron shows a similar trend, although the range of concentrations in the Bhs horizon is narrower, reaching 16 at.% Fe. In the AO horizon, only 4 out of 22 spots (18%) have detectable Fe, while in the Bh horizon more than 65% of colloids (15 out of 23 spots) contain detectable Fe. In the Bhs horizon 12 out of 29 spots (41%) have detectable Fe. In contrast, the magnitude and range of colloidal carbon concentrations are high in the AO (mostly 60–80 at.% C) and Bh (70–95 at.% C) horizons, while a wider range in the distribution of concentrations is observed in the Bhs horizon (5–90 at.% C). Both the range and values of (Al + Fe)/C atomic ratios increase with horizon depth.

Silica to aluminum ratios provide information about the type of aluminosilicate mineral present
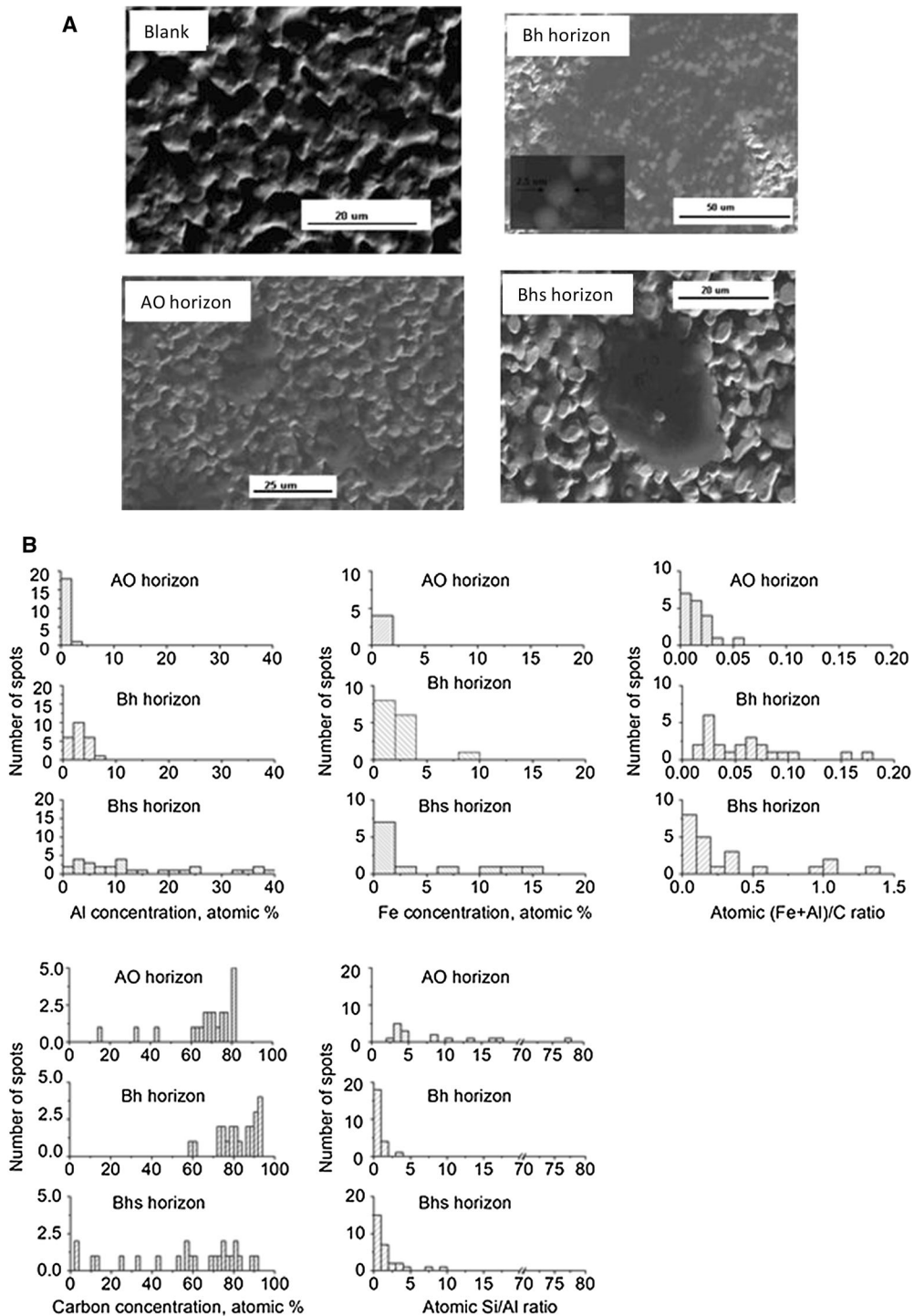
Fig. 3 a Typical SEM images of soil colloids (0.45–1.2 μm) on 0.45 μm pore size silver filters: blank filter; colloids from the AO horizon; colloids from the Bh horizon (insert are magnified particles from larger image); and colloids from the Bhs horizon showing a Fe-enriched particle embedded within the organic matrix. **b** SEM–EDS spot measurements for the AO, Bh, and Bhs horizons showing the distribution of concentrations (at.%) of Al, Fe, carbon, and (Fe + Al)/C and Si:Al ratios in soil colloids (0.45–1.2 μm). Note the scale used for x and y axes differ among panels

(Farmer and Frazer 1982; Childs et al. 1983; Yagasaki et al. 2006). The Si:Al ratios are high in the AO horizon, ranging from 2.4 to 78 (with an average of 36) which suggests the presence of colloidal silica. In the Bh horizon, Si:Al ratios are less than 1.5 for all spots but one (= 3.2), so the presence of 2:1 layer aluminosilicates is not supported. However, the presence of kaolinite is supported because 10 out of 23 spots have a Si:Al ratio close to 1 (Nagasawa 1978).

These observations are in agreement with ATR-FTIR data which indicate the presence of kaolinite in colloids from the Bh horizon (Fig. 2b). Colloids from the Bhs horizon show more heterogeneity in Si:Al ratios (0.1–7.6) and 24% of all spots have Si:Al ratios > 2 suggesting the presence of 2:1 clay minerals. This is in contrast with ATR-FTIR results that show the bulk spectrum of colloids from the Bhs horizon has a signature typical of organic components.

At a finer scale, TEM-EDS and SAED analyses show the pore water SF-L fraction from the Bh horizon (Fig. 4a–c) contains small (~ 100 nm) spherical amorphous SiO_2 particles, round organic-rich amorphous colloids ~ 2–3 μm in size with traces of Fe, Al, P and Cl, and organic-rich areas with embedded inorganic crystallites (Si > C > Fe > Ca > Al). The presence of amorphous silica colloids in the Bh horizon is in agreement with ATR-FTIR and chemical data. The presence of Fe, Al, and Si within an organic matrix implies a potential active role of organic materials in the transport of these elements through the soil profile, albeit within different structures. TEM-EDS analyses of colloids from the Bhs horizon typically show a more homogeneous organic matrix with high concentrations of Al relative to Si, Ca and Fe, and contain discrete crystallites as observed by TEM and SAED (Fig. 4d). Although an even greater number of observations is ideally needed for a more comprehensive interpretation of the TEM-EDS results (Buffle et al. 1998), these findings are in agreement with SEM–EDS data, and in particular with the ATR-FTIR spectrum of the Bhs SF-L fraction that shows a signal dominated by organic components. It is clear that mineral-organic colloidal structures are dominant associations in pore waters from subsurface Bh and Bhs illuvial horizons.

Discussion

SF-S fraction of soil pore waters

Because DOC concentrations are 100–400 times greater than metal concentrations in all horizons, and soil pH is in the range 3.4–4.3, chemical equilibrium calculations indicate that metal-DOC complexes dominate the SF-S fraction of soil pore waters from each Spodosol horizon. This result is in agreement with previous observations that DOC likely controls Fe and Al solubility in the < 0.45 μm fraction of soil pore waters, inhibiting the precipitation of secondary minerals, and increasing the mobility of these elements in soils. Our experimental results, however, also indicate the SF-S fraction of the AO horizon has the lowest (Fe + Al)/C atomic ratio and pH, and that these parameters are higher in all subsurface horizons, and highest in the Bhs horizon where the (Fe + Al)/C atomic ratio is ≈ 0.03. Increases in (Fe + Al)/C ratios with depth suggest distinct metal–organic associations are present in the SF-S fraction. To explain these findings, we propose the structure of metal–organic complexes evolves as increased amounts of metals (i.e., Al and Fe) are supplied to pore waters of increasing pH (Fig. 5). In this scenario, as metal–organic complexes travel down the soil profile they may be immobilized by the formation of Fe/Al-oxide-organic coprecipitates; i.e. initial metal complexation with organic ligands, followed by chemisorption of additional Al and Fe to metal oxygen linkages and metal hydroxide cluster formation in association with organic functional groups, and finally crystallization of mineral clusters within an organic matrix as evidenced by TEM. Increases in (Fe + Al)/C atomic ratios in the SF-S fraction may also be explained by DOC interactions with mineral colloids. DOC and related aqueous metal–organic complexes are short-lived in soils, partly due to preferential sorption onto clay-sized mineral phases (Chenu and Plante 2006; Lalonde et al. 2012; Vogel et al. 2014). Resulting DOC-mineral associations exhibit colloidal properties and can therefore serve as transport media for sorbed OC in saturated soils. Indeed, it is well established that low pH, as in a Spodosol, promotes the formation of inner-sphere bonds between DOC and variable charge mineral surfaces (Chorover and Amistadi 2001), including iron and aluminum (oxy)hydroxides and edges of clay minerals

Fig. 4 TEM, EDS and SAED data (collected for the whole area shown) of representative colloids (0.45–1.2 μm). a Bh horizon: amorphous silica colloids ∼ 100 nm in size; b Bh horizon: carbon-rich amorphous round structure containing traces of Fe and Al; c Bh horizon: organic matter with crystalline inorganic particles containing Si, Fe, Ca and Al; d Bhs horizon: amorphous organo-mineral colloids containing C and Al, and traces of Si, Ca, Fe, P and S
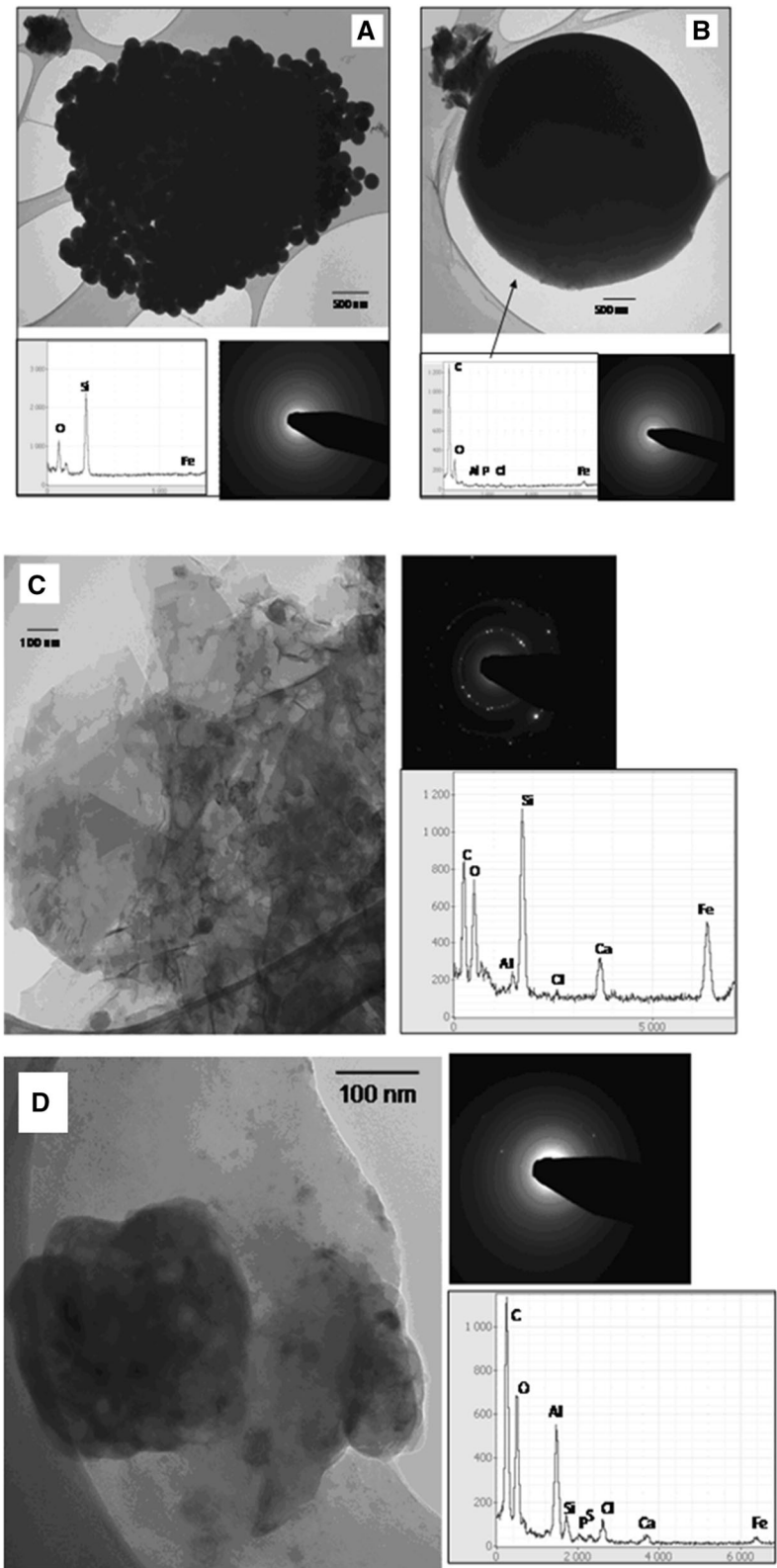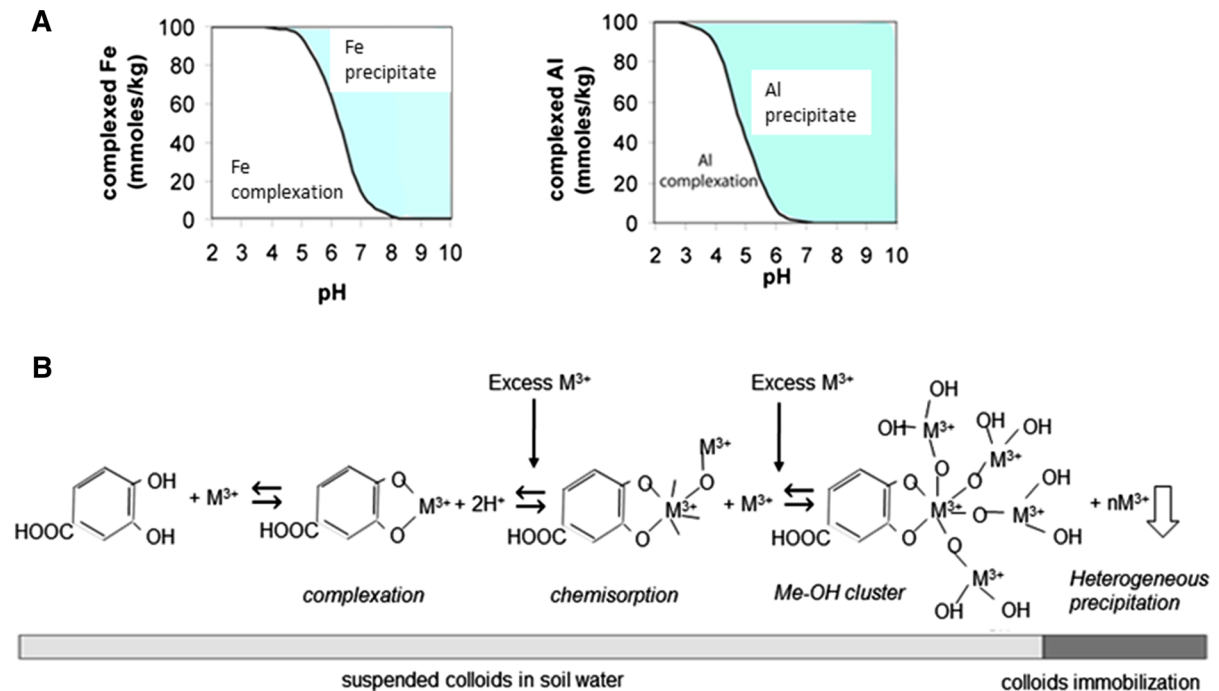
Fig. 5 Hypothesized mechanism for the accumulation of organic carbon and Fe/Al (hydr)oxides starting from species present in the SF-S fraction. **a** Predicted pH dependence of Al^{3+} and Fe^{3+} complexation with catechol-type groups of organic matter assuming $Al(OH)_3$ and $Fe(OH)_3$ control the solubility of Al and Fe, respectively (modified from McBride 1994). **b** Sequence of reactions between an organic ligand and a trivalent metal (e.g., Fe^{3+}, Al^{3+}). The organic ligand is represented by protocatechuic acid with ortho-dihydroxy functional groups, a typical phenol-type compound with the potential to form chelates with polyvalent metal ions. As the concentration (supply) of polyvalent metal cations increases, multifunctional organic-mineral colloidal structures are expected to form. These structures may eventually be immobilized when/if the Metal/C ratio in pore water increases

(Martínez-Villegas and Martínez 2008; 2012). Furthermore, the formation of DOC-mineral inner-sphere complexes is often considered slowly reversible or irreversible (Oren and Chefetz 2012) and has been shown to reduce microbial utilization of sorbed OC (Mikutta et al. 2007). Therefore, long-term transport and persistence of organic carbon within a Spodosol profile may depend on the evolution of SF-S metal–organic complexes, including growth to colloid-size particles via coprecipitation processes and interactions with mobile mineral colloids.

SF-L fraction of soil pore waters: Al, Fe, Si and organic carbon

Aluminum (Al) can be transported through soil profiles as dissolved Al-DOC complexes, and as colloidal material including Al-COC complexes, mineral colloids (e.g., Al-hydroxides, proto-imogolite, allophane, and aluminosilicate clays) and organo-mineral associations. The SF-L fraction of pore waters shows strong evidence of aluminum association with mineral colloids. ATR-FTIR spectra and/or SEM–EDS-determined Si:Al ratios support the presence of kaolinite, and possibly 2:1 clay minerals in the SF-L fraction of all Spodosol horizons. The possibility for Al transport as 2:1 aluminosilicate colloids is also inferred from the presence of vermiculite-illite in the soil clay fraction, as determined by XRD analysis. However, Al transport as amorphous aluminosilicate (i.e., proto-imogolite) seems unlikely for this Spodosol profile since the pH values of soil waters are lower than those required for proto-imogolite colloid stabilization (pH > 4.8) (Farmer and Lumsdon 2001), although the Si:Al ratios in soil colloids approximate those of imogolite (0.7–1.1). While a significant portion of Al might be transported as mineral colloids, TEM-EDS evidence indicates the association of Al with colloidal organic carbon in the Bh and Bhs

horizons where metal–organic compounds with complex structures might have formed.

The behavior of iron (Fe) in the SF-L fraction seems to depend to a great extent on the amount of organic colloids present. Iron presumably precipitates in hydroxide form more easily than aluminum since the solubility of mineral Fe phases is much lower than that of Al at pH 4-5 and the hydrolysis constant for Fe^{3+} (pK = 2.2) is higher than for Al^{3+} (pK = 5) (Stumm and Morgan [1981]). In general, Fe solubility in well-aerated soils is largely controlled by Fe-(oxy)hydroxides, Fe-organic complexes and microbial activity, the latter mostly responsible for Fe(II)/Fe(III) redox transformations (Lindsay [1991]; Riedel et al. [2013]; Colombo et al. [2015]) although abiotic Fe(II)/Fe(III) redox transformations have been shown to occur when Fe binds to various functional groups of organic matter (Bhattacharyya et al. [2013]). Sequential extractions of soil solids indicate the presence of crystalline and amorphous forms of Fe (Table [1]); however, FTIR analyses fail to detect their presence in the SF-L fraction although TEM-EDS and SEM–EDS confirm the presence of Fe in organic-rich colloids and in crystallites embedded within an organic matrix. It is possible that Fe in organic-rich colloids occurs as hydrolyzed species. For example, in a study of Fe speciation in a Spodosol soil, Gustafsson ([2009]) reported Fe-EXAFS evidence indicating hydrolyzed Fe binds to organic matter forming small iron hydroxide clusters. Visual Minteq calculations utilizing elemental concentrations from the SF-L fraction predict supersaturation with respect to iron hydroxide, thus suggesting iron hydroxide clusters could be present, but at levels below detection of the methods we use in this investigation. Furthermore, association with organic matter might prevent further growth of the presumed Fe hydroxide clusters (Seijo et al. [2009]; Bhattacharyya et al. [2018]).

Silica (Si) concentrations in the AO and Bh horizons are high and, as evidenced by SEM–EDS, TEM-EDS and infrared data, Si is transported as colloidal silica (SiO_2). Silica colloids adsorb organic matter and could therefore play an important role in its transport through soils (Jada et al. [2006]). Various mechanisms have been proposed to explain the sorption of humic substances onto silica surfaces, including electrostatic and hydrophobic attractions (Juhna et al. [2003]) and the formation of ternary complexes where polyvalent cations (i.e., Fe^{3+}, Al^{3+}) act as bridges between organic molecules and the mineral phase (Tan [2003]; Tombacz et al. [2004]). No direct unequivocal evidence for the formation of organic complexes on colloidal silica surfaces could be discerned from the work presented herein; however, correlational (Fig. [1]: concentration trends with depth) and visual (Fig. [4]c: Si-rich colloids seem to be embedded within an organic matter matrix in the Bh horizon) evidence suggests their presence. Our data provides strong evidence that Si migrates through the Spodosol profile in the form of amorphous silica and, to a lesser extent, in the form of poorly crystalline or crystalline kaolinite.

Our results support the presence of Fe, Al and Si in complexes with colloidal organic carbon (COC) and in mineral colloids embedded within COC. The stability of mineral-organic colloidal associations in pore waters is defined by chemical and electrostatic interactions between mineral particles and organic matter (Seijo et al. [2009]). In most natural systems, interactions of mineral colloids with nanometer-sized organics (e.g., proteins, DNA fragments) results in the formation of stable and mobile mineral-organic associations, while interaction with larger polymers (0.1–1 μm) destabilizes them (Buffle et al. [1998]; Seijo et al. [2009]).

Relative abundance of metals and organic matter in pore waters defines mobility of mineral-organic associations

The relative abundance of metals and organic matter (i.e., (Fe + Al)/C ratios) in soil pore waters influences the structure and size of mineral-organic associations; in addition, these ratios might be used to infer potential mechanisms of interaction. For example, dissolved metal–organic complexes aggregate to become colloids > 0.45 μm in size at (Fe + Al)/C ratios of ∼ 0.03–0.04 at pH 4–4.5 (Nierop et al. [2002]; Jansen et al. [2003]), whereas metal–organic complexes remain dissolved in soil water when (Fe + Al)/C ratios are < 0.01 (Riise et al. [2000]). Increases in (Fe + Al)/C ratios of colloidal metal–organic complexes (> 0.03) leads to neutralization of negatively charged colloidal particles by polyvalent cations, and therefore to increased polymerization, aggregation, and sedimentation of colloids. Sedimentation of colloidal particles has been shown to occur at water (Fe + Al)/C atomic ratios > 0.06 (Mckeague et al. [1971]).
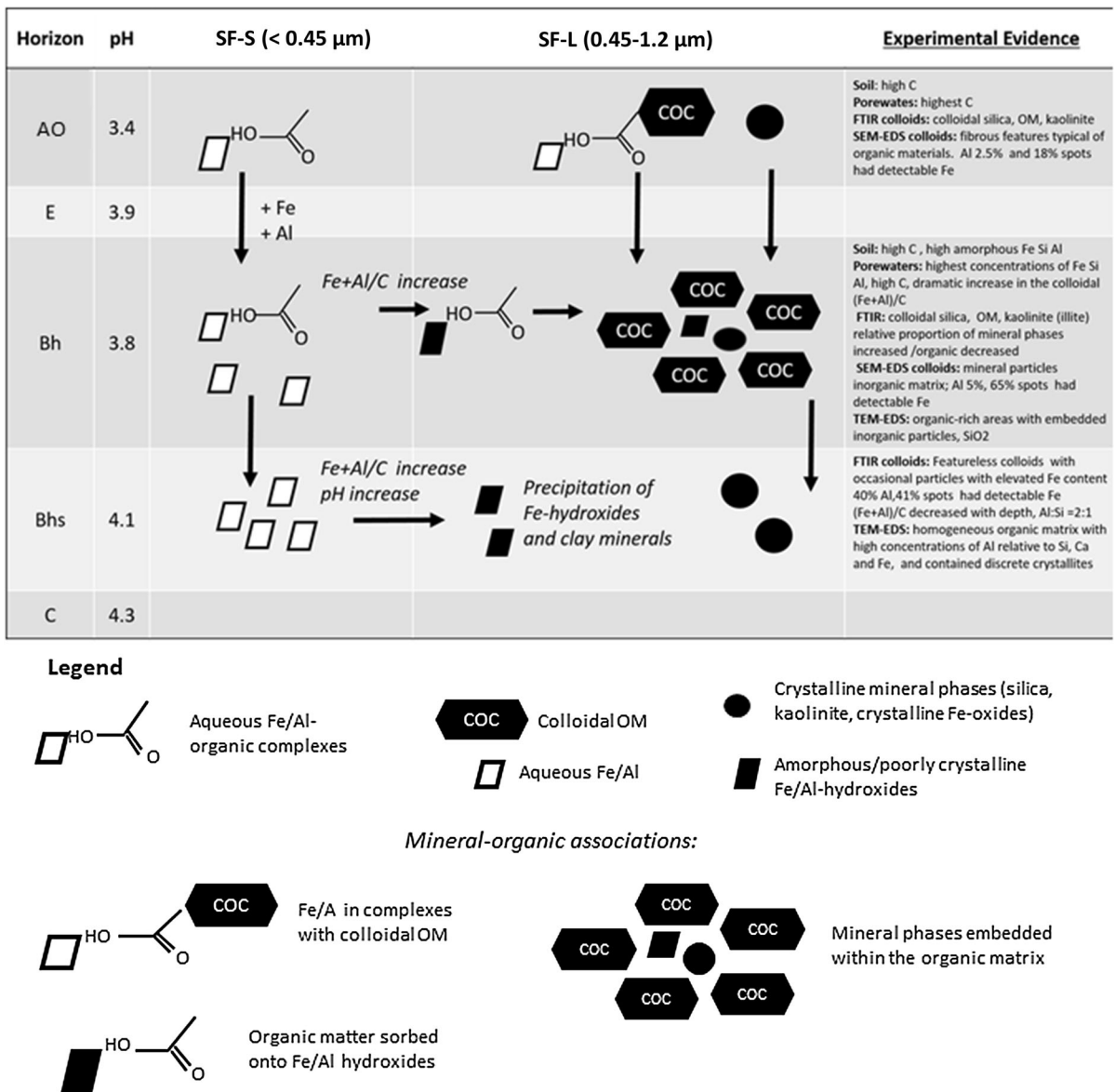
Fig. 6 Schematic diagram (not to scale) showing structures for mineral, organic and mineral-organic associations evidenced in Spodosol soil horizon pore waters, and hypothesized mechanisms for their translocation and accumulation with depth. The relative abundance of mineral-organic associations shown and their immobilization will depend on the supply of metals and organic carbon (< 0.45 and 0.45–1.2 μm size fractions) to soil pore waters, that is, on its (Fe + Al)/C ratio

In this study, the (Fe + Al)/C ratios indicate organic constituents are dominant over Al and Fe in both the SF-S (< 0.45 μm) and the SF-L (< 1.2 μm) fractions of the Spodosol pore waters (Fig. 1). Except for the SF-L fraction of the Bh horizon, the (Fe + Al)/C ratios are relatively low, ranging from 0.01 to 0.03 in the SF-S and generally lower (0.0009 to 0.004) in the SF-L fraction, which suggests high stability of both

SF-S and SF-L metal–organic associations. The (Fe + Al)/C ratio in the SF-L fraction of the Bh horizon has a value of 0.055, which is more than ten times that of other horizons. Higher (Fe + Al)/C ratios suggest immobilization of metal–organic structures in the Bh horizon, which is in agreement with chemical data showing the highest accumulation of Fe, Al, and OC in this horizon. This high (Fe + Al)/C

ratio is interpreted as saturation of COC with metal ions resulting in increased number of metal bridges that lead to polymerization of these associations in the Bh horizon. Our TEM-EDS data supports this statement as it shows mineral particles within an organic-matrix and organic matter containing Si, Al and Fe in the Bh horizon (Fig. 4a–c). In addition, the relatively high $(Fe + Al)/C$ ratio and the presence of high concentrations of amorphous materials in the Bh horizon (Table 1) indicate organic matter inhibited the formation of crystalline Fe and Al minerals, as also evidenced from previous studies (Martínez and McBride 1999). The $(Fe + Al)/C$ ratio in the SF-S fraction of the Bhs horizon is also relatively high, suggesting the formation of colloids and potential subsequent immobilization (Fig. 1). Overall, $(Al + Fe)/C$ ratios can be used to follow the evolution from dissolved metal–organic complexes to colloids dominated by Al/Fe clusters and/or precipitates. These potential pathways are schematically represented in Fig. 6. In the SF-S fraction, while DOC travels down the profile as metal-DOC complexes, they bind more Al and Fe and the $(Al + Fe)/C$ ratio increases, leading to the formation of larger colloids (> 0.45 μm) which can then precipitate/accumulate. In contrast, the SF-L fraction has much higher concentrations of COC than of Fe and Al, and therefore the $(Al + Fe)/C$ ratio is low, and remains low, except in the Bh horizon where SF-S structures evolve into SF-L structures due to increased supply of Fe and Al (Fig. 6).

Conclusions

The highest concentrations of SF-S and SF-L organic carbon and that of Fe, Al, and Si in the SF-L fraction are found in soil waters derived from the organic-rich AO and Bh horizons. Furthermore, chemical, spectroscopic and microscopic evidence indicate the SF-L fraction is primarily represented by four structures, namely, inorganic mineral colloids, OC sorbed onto mineral colloids, mineral colloids embedded within an organic matrix, and Fe/Al in complexes with colloidal OC. From these, mineral-organic associations (which may result from mechanisms such as coprecipitation, OC sorption onto mineral colloids and colloid–colloid interactions) constitute a large portion of the SF-L fraction of pore waters and seem to play a major role in their transport and accumulation. We further suggest

OC accumulation in subsurface soil horizons results from the downward movement of these colloidal structures followed by colloid immobilization due to changes in soil environment (e.g., pH, moisture, pore water composition).

In this investigation we explored methods to study short-term processes leading to colloidal transport and accumulation in Spodosols although similar structures might also contribute to the transport and availability of organic carbon in subsurface horizons of soils that range in the expression of spodic properties. Since the occurrence of the aforementioned colloidal structures in soil pore waters will depend on pH and on the relative supply of OC and Fe + Al to pore waters, information that can be readily available for most soils, our results might help to predict carbon stabilization in subsurface horizons of a variety of soil orders. Nevertheless, spodosols have the second highest average concentration of organic carbon (57.6 ± 15 g C/kg soil) in subsurface horizons among all soil orders and contribute to $\sim 5\%$ of the total carbon stored in soils (VanLoon and Duffy 2017); therefore, detailed understanding of the mechanisms of immobilization of organic carbon in Spodosols could help in predicting potential long-term changes in carbon reserves. Because interactions between mineral colloids and organic colloids in soil pore waters involve complex mechanisms, the need exists to continue to explore charging behavior, colloidal stability, and migration of mineral nanoparticles in the presence of organic matter. Moreover, since the metal/carbon ratio defines the structure and type of interaction between mineral colloids and organic matter in soil pore water, dynamic soil moisture conditions, which may affect the vertical and lateral transport of water, DOM and organo-mineral associations, must be taken into consideration.

References

Allard T, Ponthieu M, Weber T (2002) Nature and properties of suspended solids in the Amazon Basin. Bull Soc Geol Fr 173:67–75

Bailey JR, McGuire MM (2007) ATR-FTIR observations of water structure in colloidal silica: implications for the hydration force mechanism. Langmuir 23:10996–10999

Basile-Doelsch I, Balesdent J, Rose J (2015) Are interactions between organic compounds and nanoscale weathering minerals the key drivers of carbon storage in soils? Environ Sci Technol 49(7):3997–3998

Bernal B, McKinley DC, Hungate BA et al (2016) Limits to soil carbon stability; Deep, ancient soil carbon decomposition stimulated by new labile organic inputs. Soil Biol Biochem 98:85–94

Bhattacharyya A, Schmidt MP, Stavitski E, Martínez CE (2018) Iron speciation in peats: chemical and spectroscopic evidence for the co-occurrence of ferric and ferrous iron in organic complexes and mineral precipitates. Org Geochem 115:124–137

Bhattacharyya A, Stavitski E, Dvorak J et al (2013) Redox interactions between Fe and cysteine: Spectroscopic studies and multiplet calculations. Geochim Cosmochim Acta 122:89–100

Bloomfield C (1953) A study of podsolozation 1. The mobilization of iron and aluminum by scots pine needles. J Soil Sci 4:5–16

Buffle J, Wilkinson KJ, Stoll S et al (1998) A generalized description of aquatic colloidal interactions: the three-colloidal interaction approach. Environ Sci Technol 32:2887–2899

Buurman P, Jongmans AG (2004) Podzolization—an additional paradigm. Edafologia 9:107–114

Buurman P, van Reeuwijk LP (1984) Protoimogolite and the process of Spodosol formation: a critical note. J Soil Sci 35:447–452

Camino-Serrano M, Gielen B, Luyssaert S et al (2014) Linking variability in soil solution dissolved organic carbon to climate, soil type, and vegetation type. Glob Biogeochem Cycles 28(5):497–509

Chen C, Dynes JJ, Wang J et al (2014) Soft X-ray spectromicroscopy study of mineral-organic matter associations in pasture soil clay fractions. Environ Sci Technol 48(12):6678–6686

Chenu C, Plante AF (2006) Clay-sized organo-mineral complexes in a cultivation chronosequence: revisiting the concept of the 'primary organo-mineral complex'. Eur J Soil Sci 57(4):596–607

Childs CW, Parfitt RL, Lee R (1983) Movement of aluminium as an inorganic complex in some podzolised soils, New Zealand. Geoderma 29(2):139–155

Ciolkosz EJ, Thurman NC (1992) Geomorphology and soils of the Northeastern United States and Pennsylvania: a series of reprints. Agronomy department, The Pennsylvania State University, University Park

Colombo C, Palumbo G, Sellitto VM et al (2015) Stability of coprecipitated natural humic acid and ferrous iron under oxidative conditions. J Geochem Explor 151:50–56

Chorover J, Amistadi MK (2001) Reaction of forest floor organic matter at goethite, birnessite and smectite surfaces.". Geochim Cosmochim Acta 65:95–109

Christensen BT (1996) Matching measurable soil organic matter fractions with conceptual pools in simulation models of carbon turnover: revision of model structure. In: Powlson DS et al (eds) Evaluation of soil organic matter models. Springer, Berlin, pp 143–159

De Coninck F (1980) Major mechanisms in formation of spodic horizons. Geoderma 24:101–128

Di Bonito MD, Breward N, Crout N et al (2018) Chapter ten—extraction and characterization of pore water in contaminated soils. In: DE Vivo B, Belkin HE, Lima A (eds) Environmental geochemistry, 2nd edn. Elsevier, Amsterdam, pp 195–235

Dignac MF, Derrien D, Barré P et al (2017) Increasing soil carbon storage: mechanisms, effects of agricultural practices and proxies. A review. Agron Sustain Dev 37(14):1–27

Duchaufour P (1982) Pedology: pedogenesis and classification. George Allen and Unwin, London

Erich MS, Trusty GM (1997) Chemical characterization of dissolved organic matter released by limed and unlimed forest soil horizons. Can J Soil Sci 77(3):405–413

Eusterhues K, Wagner FE, Häusler W et al (2008) Characterization of ferrihydrite-soil organic matter coprecipitates by X-ray diffraction and Mossbauer spectroscopy. Environ Sci Technol 42(21):7891–7897

Farmer VC (1974) The layer silicates. The infrared spectra of minerals. Mineralogical Society, London, pp 340–349

Farmer VC, Frazer AR (1982) Chemical and colloidal stability of sols in the Al_2O_3-Fe_2O_3-SiO_2-H_2O system: their role in podzolization. J Soil Sci 33:737–742

Farmer VC, Lumsdon DG (2001) Interactions of fulvic acid with aluminum and a proto-imogolite sol: the contribution of E-horizon eluates to podzolization. Eur J Soil Sci 52:177–188

Golchin A, Oades JM, Skjemstad JO et al (1994) Soil structure and carbon cycling. Soil Res 32(5):1043–1068

Gu B, Schmitt J, Chen Z et al (1995) Adsorption and desorption of different organic matter fractions on iron oxide. Geochim Cosmochim Acta 59:219–229

Gustafsson JP (2009) MINTEQ 2.53, http://www.lwr.kth.se/english/OurSoftWare/Vminteq/index.htm

Han L, Sun K, Jin J et al (2016) Some concepts of soil organic carbon characteristics and mineral interaction from a review of literature. Soil Biol Biochem 94:107–121

Hay MB, Myneni SCB (2007) Structural environments of carboxyl groups in natural organic molecules from terrestrial systems. Part 1: Infrared spectroscopy. Geochim Cosmochim Acta 71(14):3518–3532

Hirst C, Andersson PC, Shaw S, Burke IT, Kutscher L, Murphy MJ, Maximov T, Pokrovsky OS, Mörth CM, Porcelli D (2017) Characterisation of Fe-bearing particles and colloids in the Lena River basin, NE Russia. Geochim Cosmochim Acta 213:553–573

Jada A, Akbour RA, Douch J (2006) Surface charge and adsorption from water onto quartz sand of humic acid. Chemosphere 64(8):1287–1295

Jones DL, Edwards AC (1998) Influence of sorption on the biological utilization of two simple carbon substrates. Soil Biol Biochem 30(14):1895–1902

Jansen B, Nierop KG, Verstraten JM (2003) Mobility of Fe(II), Fe(III) and Al in acidic forest soils mediated by dissolved organic matter: influence of solution pH and metal/organic carbon ratios. Geoderma 113(3):323–340

Juhna T, Klavins M, Eglite L (2003) Sorption of humic substances on aquifer material at artificial recharge of groundwater. Chemosphere 51(9):861–868

Kaiser K, Kalbitz K (2012) Cycling downwards–dissolved organic matter in soils. Soil Biol Biochem 52:29–32

Kartlun E, Bain D, Gustafsson JP et al (2000) Surface reactivity of poorly ordered minerals in podzol B horizons. Geoderma 94:236–286

Kleber M, Eusterhues K, Keiluweit M et al (2015) Chapter one: mineral-organic associations: formation, properties, and relevance in soil environments. Adv Agron 130:1–32

Kramer MG, Lajtha K, Aufdenkampe AK (2017) Depth trends of soil organic matter C: N and 15 N natural abundance controlled by association with minerals. Biogeochemistry 136:237–248

Kramer MG, Sanderman J, Chadwick OA et al (2012) Long-term carbon storage through retention of dissolved aromatic acids by reactive particles in soil. Glob Change Biol 18(8):2594–2605

Lalonde K, Mucci A, Ouellet A et al (2012) Preservation of organic matter in sediments promoted by iron. Nature 483(7388):198–200

Lindsay WL (1991) Iron oxide solubilization by organic matter and its effect on iron availability. Plant Soil 130:27–34

Lützow M, Kögel-Knabner I, Ekschmitt K et al (2006) Stabilization of organic matter in temperate soils: mechanisms and their relevance under different soil conditions—a review. Eur J Soil Sci 57(4):426–445

Lundström US, van Breemen N, Bain D (2000) The podzolization process. A review. Geoderma 94(2):91–107

Madejova J (2003) FTIR techniques in clay mineral studies. Vib Spectrosc 31(1):1–10

Martinez-Villegas N, Martinez CE (2008) Solid- and solution-phase organics dictate copper distribution and speciation in multicomponent systems containing ferrihydrite, organic matter, and montmorillonite. Environ Sci Technol 42(8):2833–2838

Martinez-Villegas N, Martinez CE (2012) Importance of dynamic soil properties in metal retention: an example from long-term cu partitioning and redistribution studies using model systems. Environ Sci Technol 46(15):8069–8074

Martínez CE, McBride MB (1999) Dissolved and labile concentrations of Cd, Cu, Pb, and Zn in aged ferrihydrite-organic matter systems. Environ Sci Technol 33:745–750

McBride MB (1994) Environmental chemistry of soils. Oxford University Press, New York

Mckeague JA, Brydon JE, Miles NM (1971) Differentiation of forms of extractable iron and aluminum in soils. Soil Sci Soc Am Proc 35:33–38

Mikutta R, Mikutta C, Kalbitz K et al (2007) Biodegradation of forest floor organic matter bound to minerals via different binding mechanisms. Geochim Cosmochim Acta 71:2569–2590

Milne CJ, Kinniburgh DG, van Riemsdijk WH, Tipping E (2003) Generic NICA-donnan model parameters for met-alion binding by humic substances. Environ Sci Technol 37:958–971

Nagasawa K (1978) Kaolin minerals. In: Sudo T, Shimoda S (eds) Developments in sedimentology, vol 26. Elsevier, Amsterdam, pp 189–219

Nierop KGJ, Jansen B, Verstraten JA (2002) Dissolved organic matter, aluminium and iron interactions: precipitation induced by metal/carbon ratio, pH and competition. Sci Total Environ 300:201–211

Oleinikova OV, Drozdova OY, Lapitskiy SA, Demin VV, Bychkov AY, Pokrovsky OS (2017) Dissolved organic matter degradation by sunlight coagulates organo-mineral colloids and produces low-molecular weight fraction of metals in boreal humic waters. Geochim Cosmochim Acta 211:97–114

Oren A, Chefetz B (2012) Sorptive and desorptive fractionation of dissolved organic matter by mineral soil matrices. J Environ Qual 41(2):526–533

Orlowski N, Pratt DL, McDonnell JJ (2016) Intercomparison of soil pore water extraction methods for stable isotope analysis. Hydrol Process 30:3434–3449

Parikh SJ, Goyne KW, Margenot AJ et al (2014) Chemical insights provided through vibrational spectroscopy. Adv Agron 126:1–112

Pokrovsky OS, Dupré B, Schott J (2005) Fe–Al–organic colloids control of trace elements in peat soil solutions: results of ultrafiltration and dialysis. Aquat Geochem 11(3):241–278

Rasmussen C, Heckman K, Biogeochemistry Wieder WR et al (2018) Beyond clay: towards an improved set of variables for predicting soil organic matter content. Biogeochemistry 137(3):297–306. https://doi.org/10.1007/s10533-018-0424-3

Riedel T, Zak D, Biester H et al (2013) Iron traps terrestrially derived dissolved organic matter at redox interfaces. Proc Natl Acad Sci USA 110(25):10101–10105

Riise G, Van Hees P, Lundstrom U et al (2000) Mobility of different size fractions of organic carbon, Al, Fe, Mn and Si in podzols. Geoderma 94:237–247

Rumpel C, Kögel-Knabner I (2011) Deep soil organic matter—a key but poorly understood component of terrestrial C cycle. Plant Soil 338(1–2):143–158

Schaetzl RJ, Anderson S (2005) Soils, paleosols, and environmental reconstruction. Genes Geomorphol, Soils, pp 632–641

Schnitzer M, Barr M, Hartenstein R (1984) Kinetics and characteristics of humic acids produced from simple phenols. Soil Biol Biochem 16:371–376

Schoenberger PJ, Wysock DA, Benham EC et al (2002) Field book for describing and sampling soils, Version 2.0. Natural Resources Conservation Service, NE

Schweigert N, Zehnder AJ, Eggen RI (2001) Chemical properties of catechols and their molecular modes of toxic action in cells, from microorganisms to mammals. Environ Microbiol 3(2):81–91

Seijo M, Ulrich S, Filela M et al (2009) Modeling the adsorption and coagulation of fulvic acids on colloids by Brownian dynamics simulations. Environ Sci Technol 43:7265–7269

Shepard JP, Mitchell MJ, Scott TJ et al (1990) Soil solution chemistry of an Adirondack Spodosol: lysimetry and N dynamics. Can J For Res 20(6):818–824

Sigfusson B, Paton GI, Gislason SR (2006) The impact of sampling techniques on soil pore water carbon measurements of an Icelandic Histic Andosol. Sci Total Environ 369:203–219

Sklemdtad JO (1992) Genesis of podzols on coastal dunes in southern Queensland. 3. The role of aluminum organic-complexes in profile development. Aust J Soil Res 30:645–665

Sposito G (1989) The chemistry of soils. Oxford University Press, New York

Stumm W, Morgan JJ (1981) Aquatic chemistry: an introduction emphasizing chemical equilibria in natural waters, 2nd edn. Wiley, New York

Tan KH (2003) Humic matter in soil and environment. Principles and controversies. Marcel Dekker, New York

Thurman EM (1985) Organic geochemistry of natural waters. Kluwer Academics Publishers, Dordrecht

Tipping E (2002) Cation binding by humic substances. Cambridge University Press, Cambridge

Tolpeshta I, Sokolova T (2009) Aluminum compounds in soil solutions and their migration in podzolic soils on two-layered deposits. Eurasian Soil Sci 42(1):24–35

Tombacz E, Libor Z, Illes E, Majzik A, Klumpp E (2004) The role of reactive surface sites and complexation by humic acids in the interaction of clay mineral and iron oxide particles. Org Geochem 35:257–267

Ugolini FC, Dawson H, Zachara J (1977) Direct evidence of particle migration in the soil solution of a podzol. Science 198:603–605

van Hees P, Lundstrom US (2000) Equilibrium models of aluminium and iron complexation with different organic acids in soil solution. Geoderma 94:201–221

VanLoon GW, Duffy SJ (2017) Environmental chemistry: a global perspective, 4th edn. Oxford University Press, Oxford

Vindedahl AM, Strehlau JH, Arnold WA et al (2016) Organic matter and iron oxide nanoparticles: aggregation, interactions, and reactivity. Environ Sci 3(3):494–505

Vogel C, Mueller CW, Hoschen C et al (2014) Submicron structures provide preferential spots for carbon and nitrogen sequestration in soils. Nat Commun 5:1–7

Wagai R, Mayer LM (2007) Sorptive stabilization of organic matter in soils by hydrous iron oxides. Geochim Cosmochim Acta 71(1):25–35

Wen LS, Warnken KW, Santschi PH (2008) Comparison between the Trinity River and the Trinity River Estuary (Galveston Bay, Texas). Mar Chem 112:20–37

Yagasaki Y, Mulder J, Okazaki M (2006) Comparing the activity of aluminum in two B horizons developed from volcanic ash deposits in Japan, dominated by short-range ordered aluminosilicates and crystalline clay minerals, respectively. Geochim Cosmochim Acta 70(1):147–163